Macromolecules

Article

Electrophoretic Stretching of DNA Molecules in Cross-Slot Nanoslit Channels

Anthony G. Balducci, Jing Tang, and Patrick S. Doyle

Macromolecules, **2008**, 41 (24), 9914-9918• DOI: 10.1021/ma8015344 • Publication Date (Web): 24 November 2008

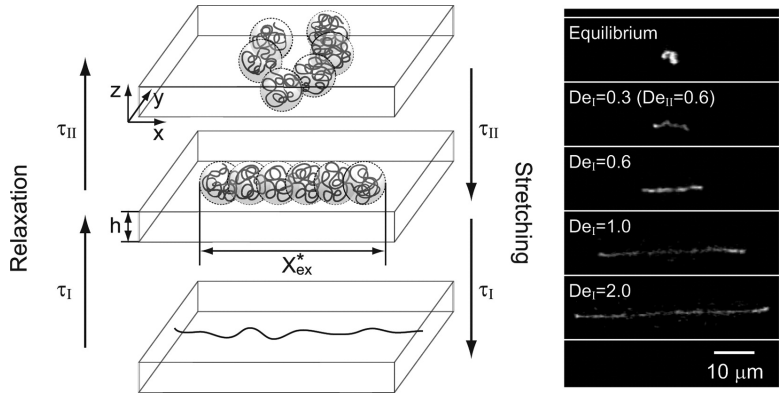

More About This Article

Additional resources and features associated with this article are available within the HTML version:

- Supporting Information
- Access to high resolution figures
- Links to articles and content related to this article
- Copyright permission to reproduce figures and/or text from this article

View the Full Text HTML

Electrophoretic Stretching of DNA Molecules in Cross-Slot Nanoslit Channels

Anthony G. Balducci,† Jing Tang,† and Patrick S. Doyle*

Department of Chemical Engineering, Massachusetts Institute of Technology, Cambridge, Massachusetts 02139

Received July 8, 2008; Revised Manuscript Received September 15, 2008

ABSTRACT: A nanofluidic cross-slot device is designed and fabricated to investigate the effects of slitlike confinement on the electrophoretic stretching of single DNA molecules. The device is capable of trapping and stretching single DNA molecules at the stagnation point of a homogeneous planar elongational electric field. Different from studies of unconfined DNA, the longest relaxation time in slitlike confinement is extension-dependent, and we find the *higher extension* relaxation time allows better prediction of the drastic increase of extension with applied strain rate in confinement. The low extension relaxation time is important in polymer rotation and small deviations from equilibrium.

I. Introduction

The development of nanofabricated devices capable of confining single DNA molecules creates the potential to alter and control the DNA shape and dynamics.[1−4] A series of recent single molecule studies have characterized DNA conformation and dynamics at equilibrium in different types of confinement, for instance, tubelike[5−10] (quasi-one-dimensional) confinement and slitlike[11−14] (quasi-two-dimensional) confinement. However, in a number of applications ranging from DNA separation[15,16] to genomic mapping,[17,18] significantly deformed molecules are important. Recently, nanoconfinement in one-dimensional (tubelike) channels has been used to create highly extended DNA of interest in particular to direct mapping methods.[5−9] Here, we report a facile method for dynamically trapping and stretching single molecules in *slitlike* nanoconfinement at a stagnation point. The molecular extensions attained here match those in the most extreme tubelike confinement, but in slitlike channels with photolithographically defined dimensions 3 orders of magnitude larger than the tubelike case. Also, since stretching the polymer can alter the interactions of the polymer with the confining walls,[19,20] the dynamics of the molecule can vary with extension, making this problem interesting from a fundamental polymer physics standpoint. Even with a recent surge in the research being done in this area (see ref 21 for a recent review), a complete understanding of polymer dynamics in confinement is lacking.

Recently, we found that in slitlike confinement the time scale governing the slowest stress relaxation of single DNA molecules depends on the molecule's extension.[20] Unlike Rouse or Zimm modes, the relaxation of the molecule very near equilibrium and at higher extensions is best described by two different time constants (see Figure 1): the low extension relaxation time τ_{II} and the higher extension relaxation time τ_I. In contrast, experiments on unconfined DNA show that a single time constant governs relaxation dynamics in the entire linear force regime (from equilibrium to ∼30% fractional extension).[22] We found that the emergence of the extension-dependent relaxation time is due to the presence of the confining walls. An initially stretched molecule is not sterically confined by the channel walls, but as it relaxes, the lateral dimensions of the molecule grow and the steric confining effects eventually become important. In a simple model which describes the polymer relaxation using a tension-blob framework (see Figure 1), the crossover point where the relaxation time changes occurs when the dimension of the blobs is equivalent to the height of the channel.[20] Before this point, relaxation happens through increasing the size of the tension blobs along the chain. During this process, the molecule is not sterically confined and the channel walls only act to alter the hydrodynamic drag through hydrodynamic screening.[23] After the crossover point, the blobs are sterically confined and can no longer grow. Here, the confining walls also change the spring force of the molecule, in addition to modulating the hydrodynamic drag. The extension at the crossover point, termed as the crossover extension (X^*_{ex}, see Figure 1), can be estimated as $X^*_{ex} = hN_{blobs}$, where h is the channel height and N_{blobs} the number of blobs. By assuming good solvent quality within blobs, a scaling relationship for X^*_{ex} was derived[20] as $X^*_{ex} \sim h^{-2/3} l_p^{1/3} w^{1/3} L_c$, where l_p, w, and L_c are the persistence length, effective width, and contour length of the DNA, respectively. The crossover extension depends on the channel height, the size of the DNA, solvent quality, and ionic strength through dependencies in w and l_p. It is important to note that both relaxation times in confinement are significantly greater than the unconfined relaxation time, pointing to the fact that confinement may allow stretching of DNA molecules at smaller deformation rates, as described below. The purpose of

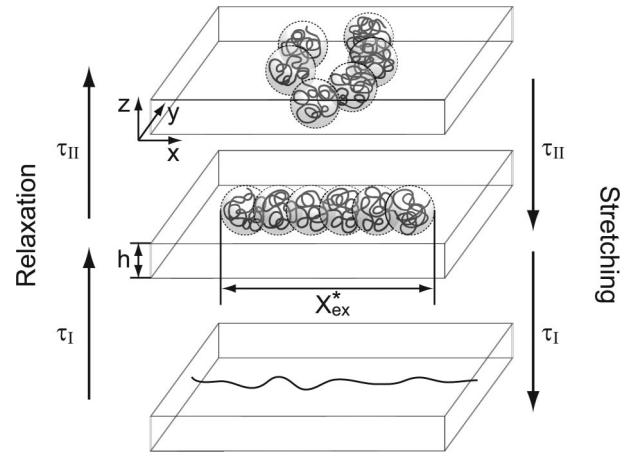

Figure 1. Schematic of the low extension relaxation time (τ_{II}) and the higher extension relaxation time (τ_I) of DNA in slitlike nanochannels and the possibility of their importance in DNA stretching. Extended molecules are no longer sterically confined and thus have different stretching and relaxation dynamics.

* Corresponding author. E-mail: pdoyle@mit.edu.
† Both authors contributed equally to this work.

10.1021/ma8015344 CCC: $40.75
Published on Web 11/24/2008

this work is to examine the effects of these newly observed relaxation physics on the electrophoretic stretching of single DNA molecules in slitlike nanoconfinement.

Polymer deformation in homogeneous extensional flows or fields is a balance of the stretching forces applied by the flow or field and the polymer's entropic elasticity tending to recoil the molecule.[24] In the unconfined case, a dimensionless group termed the Deborah number is typically used to characterize this balance. The Deborah number is defined as the product of the deformation rate of the flow or field (the strain rate $\dot{\varepsilon}$) and the polymer's longest relaxation time (τ): $De = \dot{\varepsilon}\tau$. A large change in extension with De is found[25−27] to occur near the theoretically predicted[28] critical value of $De_{crit} \approx 0.5$. The fact that the longest relaxation time is extension-dependent in slitlike confinement brings some ambiguity to the prediction of where this drastic deformation occurs. Therefore, we define two Deborah numbers for the current problem and characterize the role of each in determining the DNA behavior. $De_I = \dot{\varepsilon}\tau_I$ is defined using the higher extension relaxation time, which governs relaxation above the crossover extension X^*_{ex} to the onset of the linear force regime (~30% fractional extension). $De_{II} = \dot{\varepsilon}\tau_{II}$ is defined using the low extension relaxation time, which governs dynamics near equilibrium. The correct prediction of the required deformation rate to achieve a certain extension is important in the design of devices aiming to exploit confinement to manipulate DNA molecules.[11,29]

II. Experiments

To investigate confinement-induced changes on stretching DNA, we place single DNA molecules in homogeneous extensional electric fields under varying degrees of confinement. Electric fields are employed to move and stretch DNA because the kinematics are purely elongational at length scales larger than the Debye length (here ~ 3 nm) and deformation due to shear can be neglected.[30] In addition, electric fields are much easier to implement than pressure-driven flows for nanoscale devices. In planar elongational electrophoretic deformation, the electrophoretic velocity of a point charge varies linearly with position:

$$v_x = \mu E_x = \dot{\varepsilon} x \tag{1}$$

$$v_y = \mu E_y = -\dot{\varepsilon} y \tag{2}$$

where v_x and v_y are the velocities in the x and y directions, respectively, E_x and E_y are the electric fields in the x and y directions, respectively, μ is the electrophoretic mobility, and $\dot{\varepsilon}$ is the strain rate. Previous studies have used cross-slot[25,26,31,32] and T[27] channels to achieve these kinematic conditions. In tall channels the large spans used to create $O(100\ \mu m)$ regions of constant strain rate are not an issue. However, even slight sagging due to large spans in nanochannels affects the strength of the field and may cause pinch-off of the channel. Cross-slot nanoslit channels with the incorporation of hyperbolically curved sidewalls (see Figure 2) are implemented in this study. Since the shape of the sidewalls matches exactly the streamlines in homogeneous extensional fields, there are no inhomogeneities to disrupt the linear electric field profile over the entire intersection region.[33] This development minimizes the span needed to create $O(100\ \mu m)$ regions of homogeneous deformation. Independent control of the potential applied to the side reservoirs allows movement of the stagnation point via manually providing slight perturbations to the field.[27] These small adjustments allow the entrapment of DNA molecules at the stagnation point for very high accumulated strains (up to 50 Hencky strain units $= \dot{\varepsilon} t_{res}$, where t_{res} is the molecule's residence time in the field). Furthermore, confinement of the molecule within the focal plane ensures it remains in focus for the entire observation. (For experimental demonstration of the trapping ability of the device, see movie S1, Supporting Information.)

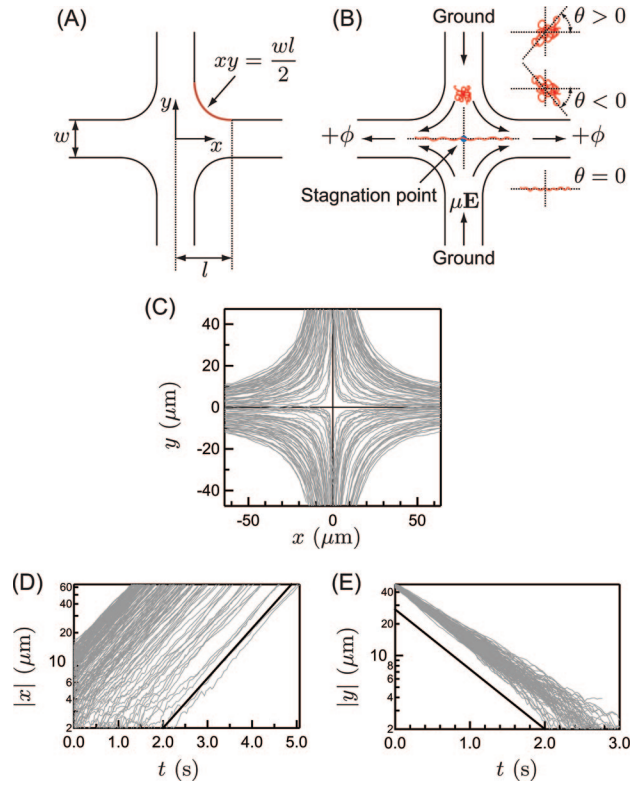

Figure 2. (A) Diagram of the cross-slot stretching device geometry. (B) Schematic of the motion and stretching of DNA molecules in the device. Independently applied voltages to the left and right arms of the channel allow adjustment of the location of the stagnation point and trapping of the DNA molecules. Also shown is the geometrical setup for the measurement of the angle of the principal axis of the radius of gyration. (C−E) Confirmation of planar elongational deformation in the center region of the 2 μm device by tracking of λ-DNA molecules (C) Trajectories of the center of mass of each λ-DNA molecule illuminate the electric field streamlines in the device. (D) and (E) display the x and y locations, respectively, of each molecule with time. The solid lines are the average of the fitted slopes of the individual traces, yielding a strain rate of $\dot{\varepsilon} = 1.2 \pm 0.1\ s^{-1}$. The relaxation time of λ-DNA in a 2 μm tall channel is $\tau_I = \tau_{II} = 0.2$ s,[30] yielding $De_I = De_{II} = 0.24 < De_{crit}$.

Channel and DNA Preparation. The channels were prepared using two methods. Microchannels ($h = 2\ \mu m$) were constructed in polydimethylsiloxane (PDMS, Sylgard 184, Dow Corning) using soft lithography on a silicon master (SU8-2 photoresist). The PDMS channels were soaked in 0.5 × Tris-borate-EDTA (TBE, Omnipure) buffer at 40 °C overnight to eliminate permeation driven flow through the PDMS,[34] rinsed and dried briefly, and sealed to a glass cover slide. Glass nanochannels with two different heights (h = 300 and 150 nm) were created by a photoresist protected etch in buffered oxide etchant and thermally bonded to a glass cover slide, as described previously.[35] The glass nanochannels were filled with filtered RO water and rinsed overnight via application of potentials at the fluid reservoirs before use. All channels were rinsed with the experimental buffer prior to exposure to DNA molecules. The buffer contained 4% β-mercaptoethanol (BME, Cabiochem) and 0.1% 10 kDa polyvinylpyrrolidone (PVP, Polysciences) in 0.5 × TBE. The experimental buffer in the glass nanochannels also incorporated a glucose (Mallinckrodt)/glucose oxidase (Roche)/catalase (Roche) (12.5, 0.16, 7.4 × 10^{-3} mg/mL, respectively) oxygen scavenging system to allow prolonged exposures required in the small channels. The channel was flushed with new buffer every 2 h during experiments to ensure a constant ionic strength environment.[36] T4GT7 DNA molecules (165.6 kbp, radius of gyration $R_{g,unconfined} = 1.46\ \mu m$,[12] Nippon gene) and λ-DNA molecules (48.502 kbp, $R_{g,unconfined} = 0.69\ \mu m$,[12] New England Biolabs) were stained with YOYO-1 (Invitrogen) dye at a basepair to dye ratio of 4:1 and allowed to sit at least overnight. The

Table 1. Channel Dimensions and T4 DNA Relaxation Times

h	τ_I (s)	τ_{II} (s)	De_{II}/De_I	l (μm)	w (μm)
2.0 μm	1.5	1.5	1	100	40
300 nm	2.7	5.4	2	50	40
150 nm	4.6	18.3	4.0	50	40

persistence length of the DNA molecules under the experimental buffer condition is $l_p \approx 53$ nm.[36] Our epifluorescence microscopy and detection setup as well as data analysis and extraction of the extension and principal axis of the radius of gyration tensor are described elsewhere.[11,20]

Electric Field Characterization. The electric field kinematics generated in the intersection region of all cross-slot devices were verified by tracking the center of mass of electrophoresing DNA under conditions in which they do not appreciably deform. λ-DNA was used as the tracer since both relaxation times (τ_I and τ_{II}) are not large enough to yield significant deformation at the electric fields employed. Figure 2C shows the center of mass position of 189 λ-DNA molecules as they electrophorese through the 2 μm tall channel. The role of the hyperbolically shaped sidewall is easily observed as no disruption to the streamlines occurs even very near the walls. Panels D and E show the experimental determination of the strain rate as the slope of the position versus time plots on semilog scales. The strain rate is indeed uniform in the intersection region of the channel, and experiments at different applied voltages confirmed that the strain rate is linear with applied electric field for all channel heights used (data not shown). The strain rate was calibrated against applied voltage prior to each experiment.

Relaxation Time Measurements. Measurement of the longest relaxation time occurred in the same channel used for the stretching experiments. A T4 DNA molecule was stretched to nearly full extension in a high field gradient at the stagnation point, the field was switched off, and the relaxation of the molecule was observed. Two distinct time constants were obtained for the two nanochannels, as expected.[20] In the 2 μm tall channel, T4 DNA is not sterically confined,[20] and thus only one time constant exists. The relaxation time was fit using the equation

$$\frac{\langle X_{ex}^2\rangle - \langle X_{ex,eq}^2\rangle}{L_c} = A\exp\left(\frac{-t}{\tau}\right) \quad (3)$$

where X_{ex} is the extension of the molecule in the stretched (x) direction, $X_{ex,eq}$ is the equilibrium extension in the stretched direction (measured after more than 10 relaxation times after turning off the field), L_c is the contour length of the T4 DNA molecule (70 μm), and t is time. A and τ are fitted parameters. Fitting regions for the two time constants are the same as those described previously.[20] Relaxation times for T4 DNA measured here are summarized in Table 1.

T4 DNA Stretching Experiments. T4 DNA was used for the stretching experiments. A typical molecule was moved into the channel intersection and allowed to rest for typically 10 longest relaxation times (τ_{II} for the nanochannels). The field was then switched on and the molecule observed for 6 min or at least 20 units of strain. The time constraint is to limit photobleaching of and photoinduced damage to the stained DNA molecules. The extension of the molecule in the x-direction (X_{ex}) was measured via a simple threshold. Steady-state averages were obtained by sampling individual traces at time intervals equal to the higher extension relaxation time τ_I after the molecule has experienced a strain of 10 (except for the case of $De_I = 0.1$ in the 150 nm tall channel, a strain of 5 was used because 10 units of strain cannot be attained under this very small applied strain rate due to the observation time constraint). Ensemble averages were taken over at least 10 molecules (at the lowest strain rates) to more than 50 (at the highest strain rates).

III. Results and Discussion

Figure 3A shows the fractional extension (normalized by the contour length) with strain for individual molecules (gray lines)

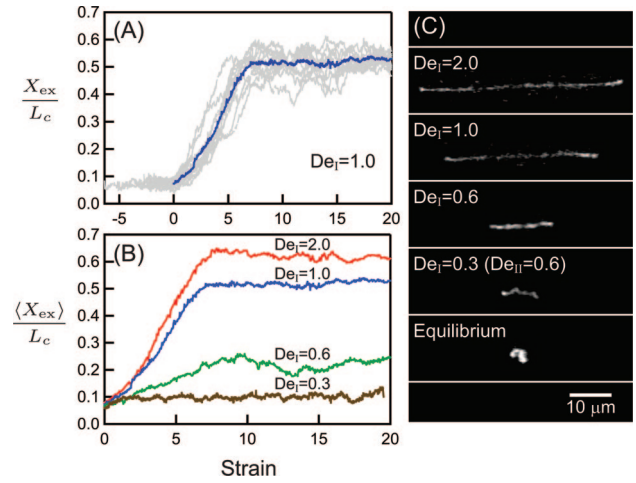

Figure 3. (A) Gray lines indicate individual traces of the fractional extension of each molecule versus strain applied (residence time in the field times the strain rate) for $De_I = 1$ in a 300 nm tall channel. The bold line is the ensemble average extension with strain. (B) Ensemble average extension as a function of strain for selected De_I in the 300 nm tall device. (C) Snapshots of individual DNA images at steady state at the given De_I in the 300 nm tall device.

as well as their ensemble-average (bold line) for the 300 nm tall channel at $De_I = 1$. Figure 3B shows the ensemble-average extension for four De_I in the 300 nm tall channel. It is clearly observed, even for low De_I, that the molecules reach steady state after an applied strain on order 10. Thus, the trapping ability and residence times afforded by our device is sufficient for experimental observation of the steady-state stretch at these deformation rates. The fact that steady state is reached after ~10 units of strain is interesting in its own right. This is the same order of magnitude as observed in studies of unconfined DNA,[37] implying that while confinement may alter the level of stretch that can be attained at a given strain rate, it does not necessarily significantly increase the rate of stretching. More careful studies focusing on the stretching transients are needed to fully characterize these effects.

Figure 4 shows the steady-state extension versus dimensional and nondimensional measures of the strength of the deformation applied. Figure 4A shows very clearly that confinement does indeed aid DNA stretching. The stretch increases at a given strain rate with decreasing channel height, more than 7-fold between the 2 μm and 150 nm tall devices at a strain rate of 0.2 s^{-1}. Importantly, at high extensions, the strain rate required to achieve a given extension can be decreased by more than 70% by exploiting confinement at these scales.

Figure 4B displays the same steady-state average extension versus De_{II}, the Deborah number using the low extension relaxation time (τ_{II}) to normalize the strain rate. The data do not collapse, and the location where the large increase in extension occurs does not agree with the predicted value of $De_{crit} = 0.5$. We conclude that the low extension relaxation time does not govern the coil−stretch transition in slitlike confinement. These results are in accord with our previous data[20] where the dynamics of relaxation are governed by the low extension relaxation time only very near equilibrium. We will return to this point below.

Figure 4C displays the steady-state average extension versus De_I, the Deborah number using the higher extension relaxation time to normalize the strain rate. It is clearly seen that this second slow time scale collapses the data quite well, and the drastic increase in extension occurs at approximately $De_I = 0.5$. The coil−stretch transition and stretch at higher extensions are better described by the second-longest relaxation time, a phenomenon unique to confinement in polymer physics. This

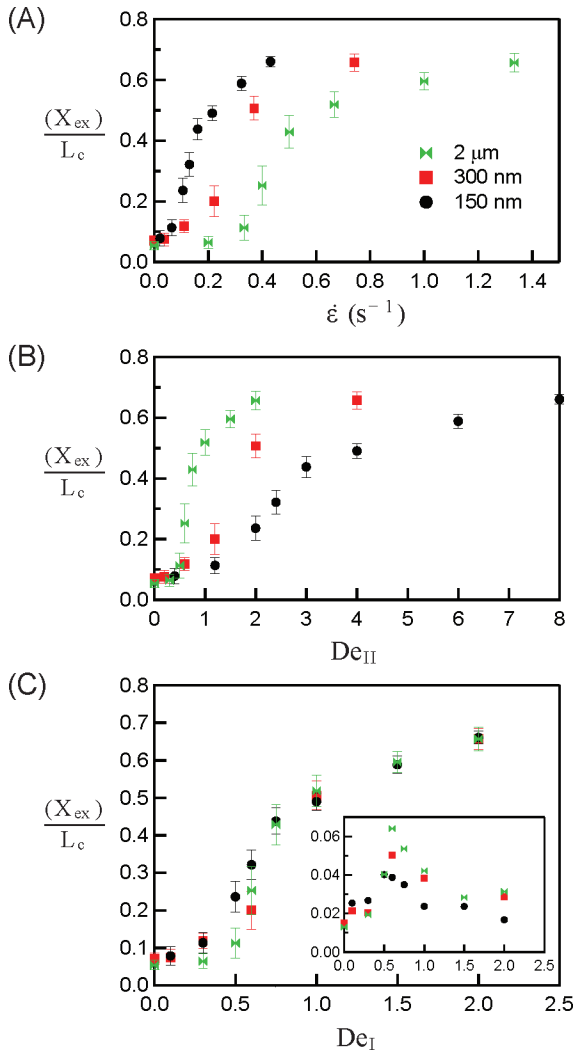

Figure 4. (A) Ensemble average steady-state extension versus the dimensional strain rate for three channel heights. (B) Ensemble average steady-state extension versus De_{II}, the strain rate normalized by the low extension relaxation time. (C) Ensemble average steady-state extension versus De_I, the strain rate normalized by the higher extension relaxation time. Inset: standard deviation (σ/L_c) of the steady-state stretch versus De_I.

data collapse is also seen in the inset of Figure 4, where the standard deviation of the average extension (σ/L_c) is plotted against De_I. Recent studies[38] have shown that the peak in this plot is a very good indicator of the location of the coil−stretch transition, and here we note that the peak is well-aligned on the abscissa. This alignment confirms that the higher extension relaxation time governs the large increase in the stretch of the molecule with applied strain rate. This finding provides a fundamental basis for the design of devices aiming to utilize slitlike confinement to attain highly extended DNA molecules. In these devices the higher extension relaxation time (τ_I) is the correct time scale that should be used for the prediction of the deformation rates required to achieve certain extensions because τ_I allows data collapse in the high extension regime.

However, at low De_I, Figure 4C does show some differences in steady-state extension between the three channel heights. Specifically, the coil−stretch transition becomes more gradual in the more confined channels: we observe significant stretching at subcritical $De_I < 0.5$, but where $De_{II} > 0.5$ (see Figure 3C, also see movie S2 and movie S3, Supporting Information). The more gradual transition may also account for the decreasing amplitude of the peak in the standard deviation with De_I plot

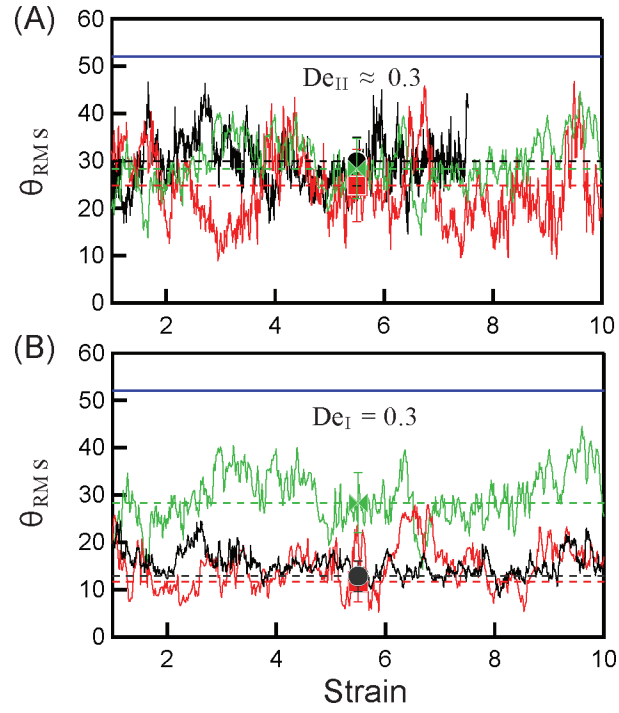

Figure 5. (A) Root-mean-square angle of the principal axis of the radius of gyration relative to the x-axis (θ_{RMS}, in degrees) versus strain for $De_{II} \approx 0.3$ for the three channel heights. Green, red, and black solid lines denote the 2 μm, 300 nm, and 150 nm tall channels, respectively; colored dashed lines and markers denote the steady-state ensemble average RMS angle. $De_{II} = 0.3$, 0.2, and 0.4 for the 2 μm, 300 nm, and 150 nm channels, respectively. The horizontal solid line denotes the equilibrium average ($\theta_{RMS,eq} = 52°$). (B) θ_{RMS} for the three channel heights for $De_I = 0.3$, corresponding De_{II} is 0.3, 0.6, and 1.2 for the 2 μm, 300 nm, and 150 nm channels, respectively.

(inset of Figure 4C).[38] As expected, τ_{II} appears to affect stretching at low extensions, below the predicted relative crossover extensions[20] of $X^*_{ex}/L_c = 0.17$ and 0.27 for the 300 and 150 nm tall channels, respectively. Note that these predicted crossover extensions overestimate the region governed by τ_{II} because they predict the center of a gradual transition.[20] Since the changes of steady-state extensions involved here are small, it is helpful to examine other indicators of behavior departing from equilibrium dynamics.

Figure 5 shows the root-mean-square angle (θ_{RMS}) of the principal axis of the in-plane DNA radius of gyration (see Figure 2) as a function of strain. θ_{RMS} indicates the degree of orientation toward the axis of elongation (x-axis, $\theta_{RMS} = 0°$) from the equilibrium average of $\theta_{RMS,eq} = 52°$ (the horizontal solid line in Figure 5). The angle reaches steady state at relatively low strain and fluctuates about the average. Figure 5A shows ensemble-average θ_{RMS} traces and the steady-state averages for the three channel heights at similar subcritical De_{II} (≈0.3). The data collapse well, and DNA molecules in three channel heights all show a similar degree of orientation. All three traces show clear orientation from equilibrium, suggesting that θ_{RMS} can provide a strong measurable signal even very near equilibrium. Figure 5B shows the same quantities for the three channel heights at the same De_I (=0.3). Data collapse is not as good, and DNA molecules in the two nanochannels display significantly more orientation than those in the 2 μm tall channel. This observation is consistent with the fact that although De_I is subcritical for all channel heights in Figure 5B, De_{II} are above 0.5 for the two nanochannels (0.6 and 1.2 for the 300 and 150 nm tall channels, respectively). Thus, the low extension relaxation time (τ_{II}) more adequately describes behavior close to equilibrium and should be used to predict the first deviations from equilibrium.

IV. Conclusions

We have designed a cross-slot device which yields large regions of homogeneous extensional deformation with limited spans amenable to the nanofluidic environment. Thus, we are able to exploit changes to the polymer dynamics induced by nanoslit confinement in order to facilitate dynamic manipulation of single molecules. We are able to easily select, trap, and stretch individual DNA molecules to steady state in this device. The confinement ensures the entire molecule remains in focus during the process, unlike other much taller microfluidic stretching devices.[25,26,31,32,39] From the stretching results presented here, we conclude that confinement does aid the stretching of single DNA molecules by allowing the use of much smaller strain rates to achieve the same amount of extension. However, the time scale governing the large change in extension with applied strain rate is the higher extension relaxation time (τ_I). This finding is important since the prediction of this transition often forms the crux of design specifications for processes involving stretching or deforming DNA molecules, and naive application of unconfined theory to confined systems would significantly underpredict the strain rates required to deform DNA molecules. The low extension relaxation time (τ_{II}) governs the orientation and small deviations from equilibrium of the molecule. Our results are important for future studies of DNA dynamics in confinement, especially those concerned with the measurement of relaxation times or dynamic manipulation of extended DNA.

Acknowledgment. The authors thank NSF Career Grant CTS-0239012, Singapore-MIT Alliance for Research and Technology (SMART), and U.S. Genomics for funding.

Supporting Information Available: Movie of demonstration of trapping and stretching of T4 DNA molecules; movies comparing steady-state extension of T4 DNA in different channel heights at same De_I. This material is available free of charge via the Internet at http://pubs.acs.org.

References and Notes

(1) Brochard, F.; de Gennes, P. G. *J. Chem. Phys.* **1977**, *67*, 52.
(2) Brochard, F. *J. Phys. (Paris)* **1977**, *38*, 1285.
(3) Daoud, M.; de Gennes, P. G. *J. Phys. (Paris)* **1977**, *38*, 85.
(4) Odijk, T. *Macromolecules* **1983**, *16*, 1340.
(5) Reisner, W.; Morton, K. J.; Riehn, R.; Wang, Y. M.; Yu, Z.; Rosen, M.; Sturn, J. C.; Chou, S. Y.; Frey, E.; Austin, R. H. *Phys. Rev. Lett.* **2005**, *94*, 196101.
(6) Jo, K.; Dhingra, D. M.; Odijk, T.; de Pablo, J. J.; Graham, M. D.; Runnheim, R.; Forrest, D.; Schwartz, D. C. *Proc. Natl. Acad. Sci. U.S.A.* **2007**, *104*, 2673.
(7) Douville, N.; Huh, D.; Takayama, S. *Anal. Bioanal. Chem.* **2008**.
(8) Guo, L. J.; Cheng, X.; Chou, C. F. *Nano Lett.* **2004**, *4*, 69.
(9) Mannion, J. T.; Reccius, C. H.; Cross, J. D.; Craighead, H. G. *Biophys. J.* **2006**, *90*, 4358.
(10) Zhang, C.; Zhang, F.; van Kan, J. A.; van der Maarel, J. R. C. *J. Chem. Phys.* **2008**, *128*, 225109.
(11) Hsieh, C.-C.; Balducci, A.; Doyle, P. S. *Macromolecules* **2007**, *40*, 5196.
(12) Balducci, A.; Mao, P.; Han, J.; Doyle, P. S. *Macromolecules* **2006**, *39*, 6273.
(13) Lin, P. K.; Fu, C. C.; Chen, Y. L.; Chen, Y. R.; Wei, P. K.; Kuan, C. H.; Fann, W. S. *Phys. Rev. E* **2007**, *76*, 8.
(14) Krishnan, M.; Monch, I.; Scwille, P. *Nano Lett.* **2007**, *7*, 1270.
(15) Han, J.; Craighead, H. *Science* **2000**, *288*, 1026.
(16) Doyle, P. S.; Bibette, J.; Bancaud, A.; Viovy, J.-L. *Science* **2002**, *295*, 2237.
(17) Larson, J. W.; Yantz, G. R.; Zhong, Q.; Charnas, R.; D'Antoni, C. M.; Gallo, M. V.; Gillis, K. A.; Neely, L. A.; Phillips, K. M.; Wong, G. G.; Gullans, S. R.; Gilmanshin, R. *Lab Chip* **2006**, *9*, 1187.
(18) Schwartz, D. C.; Li, X.; Hernandez, L. I.; Ramnarain, S. P.; Huff, E. J.; Wang, Y.-K. *Science* **1993**, *262*, 110.
(19) Brochard-Wyart, F. *Europhys. Lett.* **1993**, *23*, 105.
(20) Balducci, A.; Hsieh, C.-C.; Doyle, P. S. *Phys. Rev. Lett.* **2007**, *99*, 238102.
(21) Hsieh, C.-C.; Doyle, P. S. *Korea-Australia Rheol. J.*, **2008**, *20*, 127.
(22) Perkins, T.; Quake, S.; Smith, D.; Chu, S. *Science* **1994**, *264*, 822.
(23) Balducci et al., A. *Macromolecules* **2006**, *39*, 6273.
(24) de Gennes, P. G. *J. Chem. Phys.* **1974**, *60*, 5030.
(25) Perkins, T.; Smith, D.; Chu, S. *Science* **1997**, *276*, 2016.
(26) Smith, D.; Chu, S. *Science* **1998**, *281*, 1335.
(27) Tang, J.; Doyle, P. S. *App. Phys. Lett.* **2007**, *90*, 224103.
(28) Larson, R. G.; Magda, J. J. *Macromolecules* **1989**, *22*, 3004.
(29) Bakajin, O. B.; Duke, T. A. J.; Chou, C. F.; Chan, S. S.; Austin, R. H.; Cox, E. C. *Phys. Rev. Lett.* **1998**, *80*, 2737.
(30) Randall, G. C.; Doyle, P. S. *Macromolecules* **2005**, *38*, 2410.
(31) Schroeder, C.; Babcock, H.; Shaqfeh, E.; Chu, S. *Science* **2003**, *301*, 1515.
(32) Juang, Y.-J.; Wang, S.; Hu, X.; Lee, L. J. *Phys. Rev. Lett.* **2004**, *93*, 268105.
(33) Deen, W. M. *Analysis of Transport Phenomena*; Oxford University Press: New York, 1998.
(34) Randall, G. C.; Doyle, P. S. *Proc. Natl. Acad. Sci. U.S.A.* **2005**, *102*, 10813.
(35) Mao, P.; Han, J. *Lab Chip* **2005**, *5*, 837.
(36) Hsieh, C.-C.; Balducci, A.; Doyle, P. *Nano Lett.* **2008**, *8*, 1683.
(37) Larson, R. G. *J. Non-Newtonian Fluid Mech.* **2000**, *94*, 37.
(38) Gerashchenko, S.; Steinberg, V. *Phys. Rev. E* **2008**, *78*, 040801 (R).
(39) Lee, J. S.; Shaqfeh, E. S. G.; Muller, S. J. *Phys. Rev. E* **2007**, *75*, 040802(R)

MA8015344